CST simulations of THz Smith-Purcell radiation from a lamellar grating with vacuum gaps

K. Lekomtsev [a1], P. Karataev [b], A. A. Tishchenko [c] and J. Urakawa [a]

[a] High Energy Accelerator Research Organization (KEK), 1-1 Oho, Tsukuba, Ibaraki 305-0801, Japan

[b] John Adams Institute at Royal Holloway University of London, Egham, Surrey TW20 0EX, UK

[c] National Research Nuclear University MEPhI, Kashirskoe sh. 31, Moscow 116409, Russia

Abstract Smith-Purcell radiation (SPR) from a lamellar grating with vacuum gaps was calculated using Computer Simulation Technology (CST) Particle In Cell (PIC) solver. The shapes of the radiation distributions were compared with those of Resonant Diffraction Radiation theory. Study of calculation domain meshing was performed. Influence of a transverse bunch size on the calculation accuracy and an SPR intensity distribution was investigated. Dependencies of the SPR yield on Lorentz factor and grating strip depth were calculated and compared with previously reported theoretical and experimental studies.

Keywords: Electromagnetic simulations, THz radiation, Smith-Purcell radiation

1. Introduction

Terahertz spectral range covers the frequency region from 0.3 to 10 THz. Electromagnetic radiation in this region has many existing and potential applications in the areas of spectroscopy, imaging, and security [1]. Chemical and physical systems experiencing change demonstrate spectral signatures in this part of electromagnetic radiation spectrum. This has led to the development of time-resolved spectroscopic tools across this entire range. THz radiation can be used to study dynamics in nanoscale physical systems such as nanotubes and single-monolayer graphene sheets. Low THz radiation can also be applied to screening of concealed explosives because they exhibit high transmission through many nonconductive materials, including concrete, clothing, and paper. THz frequency region is very challenging part of electromagnetic spectrum for radiation generation and detection because of relatively low maturity level of components and systems that operate in this region. Although situation is improving with more and more advances in the field, much of challenging and exciting potential still remains untapped [2].

Recent advances in generation of short (hundreds of femtoseconds) pre-bunched beams have a potential to generate coherent THz radiation with high signal-to-noise ratio occurring via Smith-Purcell radiation (SPR) from diffraction grating in super-radiant regime. SPR arises as a result of interaction between the field of an electron bunch travelling in the vicinity of a periodic target with the target material. For a relativistic electron bunch with longitudinal dimension σ_{long} and a grating with period p coherent SPR occurs when the wavelength of radiation satisfies the condition $\sigma_{long} \ll \lambda \leq 2p/m$, where m is a diffraction order, the radiation intensity becomes proportional to the square of electron current [3]. Super-radiant regime takes place when SPR from a periodic train of bunches is locked to the train frequency in discrete harmonics. In the super-radiant regime the radiation intensity measurements of frequency locked coherent SPR in sub-THz frequency region were demonstrated in [4, 5]. Currently LUCX accelerator at High Energy Accelerator Research Organisation (KEK) is being upgraded by introducing femtosecond Ti:Sa laser system and ultimately it will generate short few tens of femtosecond electron bunches [6, 7].

In this report we present simulations of SPR from a lamellar grating with vacuum gaps, which is being considered for an experimental study at LUCX facility. The simulations are performed in Computer Simulation Technology (CST) Particle Studio (PS) software package. The study of Transition Radiation using Particle In Cell (PIC) solver of CST PS was discussed in [8], the methodology for the fields computation and propagation using this solver was presented in [8, 9, 10, 11]. The main motivation for this work is to study CST PS as a tool for SPR grating optimisation and for pre-experimental validation of the grating parameters. In this report angular intensity distributions of SPR will be compared with the Resonant Diffraction Radiation theory developed in [12]. Effects of meshing and the calculation errors they introduce will be estimated. Radiation intensity dependencies on a grating groove depth as well as a bunch energy and transverse size will be considered.

[1] konstlek@post.kek.jp; +81 80 3177 9993

2. Calculation geometry.

A geometry considered in CST simulation is shown in Figs 1-3. Perfect Electric Conductor (PEC) set of strips is located in the calculation domain filled with vacuum. Fig. 1 shows a top view of the geometry with the cross-section by Oxz plane. Angle Theta corresponds to the polar angle of radiation observation. An electron bunch travels close to the grating with the impact parameter h along the +z direction. Fig. 2 shows a side view of the geometry and depicts grating width (w2), grating period (p), and strip width (w1).

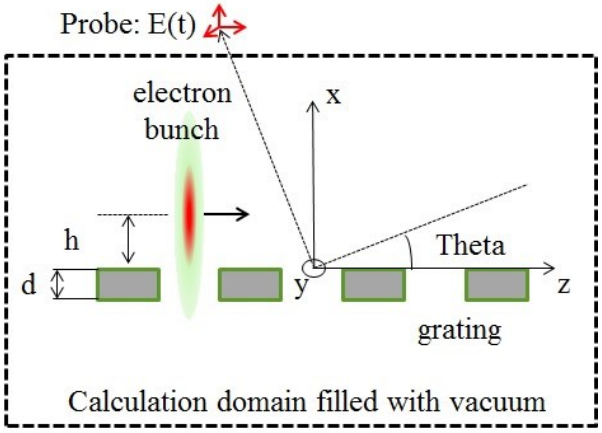

Fig. 1 Top view of the geometry. The beam propagates along the +z direction.

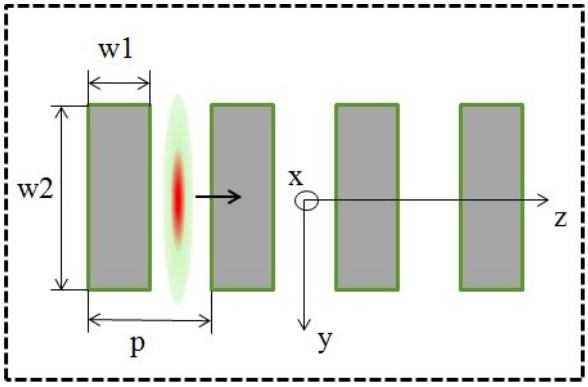

Fig. 2 Side view of the geometry.

Fig. 3 shows a front view of the geometry, electron bunch travels towards an observer in the vicinity of the grating. Angle Phi is azimuthal angle of radiation observation. Table 1 shows the parameter ranges used in the simulations.

Radiation intensity pattern is calculated from the grating acting as a radiation emitter after the bunch has passed by the target. Electric field values are calculated in the calculation domain at each point of the mesh for a given discretization. The field values corresponding to the far-field are calculated from the electric field values at the border of the calculation domain by extrapolation, using the techniques described in [13]. Boundary conditions are chosen to be open, so there are no additional reflections introduced by the borders of the calculation domain.

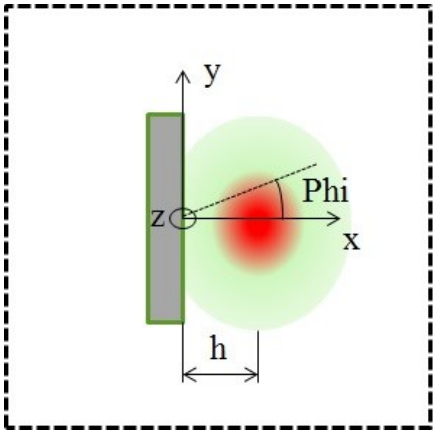

Fig. 3 Front view of the geometry. The beam propagates in the +z direction.

Parameter	Value
Bunch energy (γ)	5 – 40
Bunch charge	0.1 nC
Bunch longitudinal size, RMS width (σ_{long})	0.1 mm
Bunch transverse size, RMS width (σ_{transv})	Point-like or σ_{transv}
Radiation frequency / wavelength	450 - 700 GHz / 0.43 - 0.67 mm
Grating material	Perfect Electric Conductor
Number of strips	20
Strip width (w1)	0.2 mm
Grating period (p)	0.4 mm
Grating width (w2)	10 mm
Strip depth (d)	0.04 – 1 mm
Impact parameter (h)	0.3 – 0.7 mm

Table 1 Grating and bunch parameters.

Smith-Purcell radiation (SPR) arises due to interaction of electric field of a bunch with the strips' material, and the radiation distribution follows the SPR dispersion relation [3]:

$$\lambda_n = \frac{d}{n}\left(cos\theta - \frac{1}{\beta}\right); \quad (1)$$

where λ_n is an observation wavelength, d is the grating period; θ is the polar angle shown in Fig. 1; $\beta = v/c$ is the speed of electron bunch in terms of the speed of light; $n = -1, -2, -3 \ldots$ is a diffraction order. For all simulations shown in this paper the diffraction order was chosen to be $n = -1$.

3. Results and Discussion.

3.1 Comparison with the Resonant Diffraction Radiation theory.

Simulated radiation distributions were compared with the Resonant Diffraction Radiation (RDR) theory developed in [12]. The theory was developed for a set of thin, ideally conducting, and infinite in the direction of the axis y (see Fig. 2) strips separated by vacuum gaps.

In [12] spectral-angular distribution of resonant diffraction radiation on strips was calculated in the following way:

$$\frac{d^2W_{RDR}}{d\omega d\Omega} = \frac{d^2W_{DR}}{d\omega d\Omega} F_2 F_3; \quad (2)$$

where $\frac{d^2W_{DR}}{d\omega d\Omega}$ is a spectral-angular distribution of the diffraction radiation from a half-plane; F_2 is the factor describing interference fields from the "input" and "output" boundaries of a strip; F_3 is the factor describing interference from *N* identical elements of the grating.

Fig. 4 and 5 show on a relative scale comparison of the theoretical curves with the CST simulation of thin ($\mathrm{str.dep.} \ll \lambda$), ideally conducting strips, which are limited in size along the direction of the axis y. The simulated curve for the polar SPR distribution agrees well with the theoretical curve. In Fig. 4 the peak's position and width correspond to the theoretical curve.

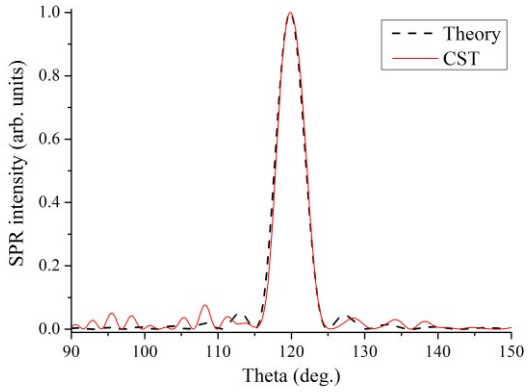

Fig. 4 Polar distribution of SPR. Phi = 0 and Theta is in the range (90; 150) deg. The following parameters were used: σ_{transv} is point-like; γ = 16; d = 0.1 mm; h = 0.7 mm.

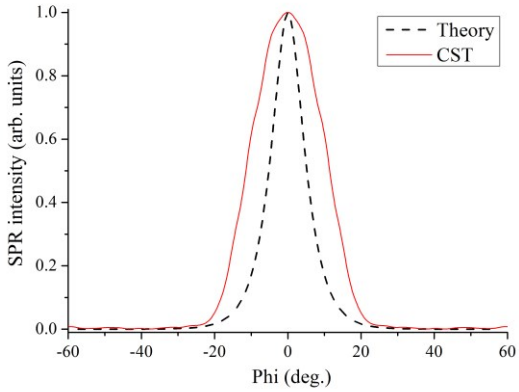

Fig. 5 Azimuthal distribution of SPR. Theta = 119.87 deg. ($n = -1$ diffraction order) and Theta is in the range (-60; 60) deg. The following parameters were used: σ_{transv} is point-like; γ = 16; d = 0.1 mm; h = 0.7 mm.

However, the simulated azimuthal distribution in Fig. 5 demonstrates widening of the radiation distribution, when compared to the theoretical curve. Discrepancies between the simulation and the theory may be caused by a meshing error, which is discussed in section 3.2, or by the geometrical differences between the theoretical and the simulated geometry. The theory was developed for infinitely thin and long strips (in the axis y direction). In the simulation the strip depth was chosen to be 0.1mm, which is six times smaller than the considered

wavelength and gives a reasonable approximation of thin strips. However, in the simulation the grating width was chosen to be approximately equal to the parameter $\gamma\lambda$ in order to capture the main part of the electric field created by the bunch in the Oxy plane (see Fig. 3). This difference in the geometries considered in the theory and the simulation may contribute in widening of the radiation distribution in Fig. 5.

3.2 Meshing study

In order to understand better how accurate CST performs calculations, depending on a chosen discretization, separate study based on the calculation of spectra was performed. Fig. 1 shows the calculation domain and a probe which is positioned outside the domain. The probe was located in the Oxz plane at the angle Theta corresponding to the first diffraction order ($n = -1$) of the considered grating. At each calculation step the probe records azimuthal (E_{Phi}), polar (E_{Theta}), and absolute ($\sqrt{E_{Phi}^2 + E_{Theta}^2}$) values of the extrapolated electric field. By performing Fourier transform of the absolute electric field dependence on time, spectra for various meshing strategies may be obtained.

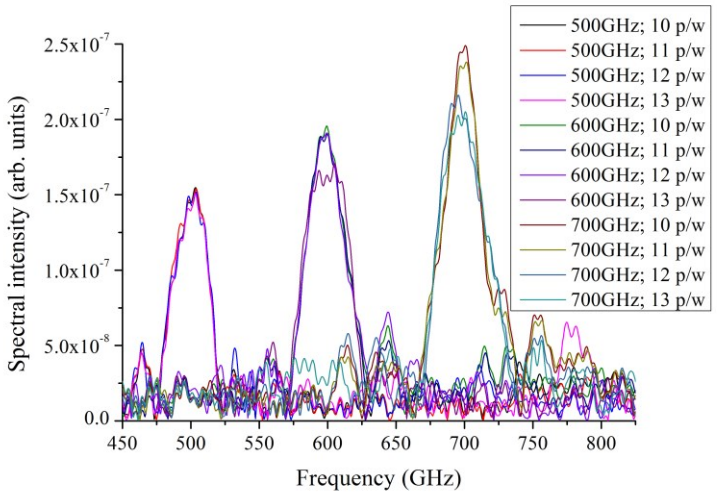

Fig 6 Spectra of SPR. Parameters: Phi = 0; Theta at probe locations corresponding to the diffraction order $n = -1$ of 500, 600 and 700 GHz; σ_{transv} is point-like; γ = 16; d = 0.1 mm; h = 0.7 mm.

Fig. 6 shows spectra recorded by the probe for three wavelengths 0.6, 0.5, and 0.43 mm (corresponding to 500, 600, and 700GHz) and for four meshing strategies 10, 12, 13, 14 p/w, where index (p/w) means (points per smallest considered wavelength). Electric field probe is located at 150 mm from the center of the grating, which roughly corresponds to the parameter $\gamma^2\lambda$. The wavelength range 0.36 to 0.66 mm (frequency range 450 to 825 GHz) was considered in the simulation; therefore the best mesh discretization ratio corresponded to 13 points per 0.36mm.

All the grating parameters were fixed and only the value of discretization ratio was changed. One may see that spectra for the frequency 500GHz are reproduced very well, however the higher the considered frequency the more difficult it becomes to reconstruct spectrum reliably. For the highest frequency 700GHz the spectral intensity value varies considerably for four different discretization ratios. Spectra calculations and radiation distribution calculations are directly connected in the CST simulations, because the same electric field values are used for both spectra and radiation distribution calculations. The distributions shown in Fig. 4 and 5 in section 3.1 were calculated for the best possible discretization ratio of 13 point per 0.36mm. Majority of the results shown in the sections 3.3, 3.4 were obtained for the value of the discretization ratio approximately equal to 10 points per 0.36mm and the frequency of 500GHz; since it was confirmed that even relatively coarse discretization gives a reliable spectral intensity value for this frequency, which is not changed by the increase of the discretization ratio.

3.3 SPR intensity dependence on the size of emission source

For the calculations described in sections 3.1 and 3.2 a point-like approximation was used for the charge distribution in the transverse plane. However, CST allows defining the transverse distribution of bunch charge using Gaussian function. In order to define a transverse Gaussian bunch one has to choose a number of emission points, the more points are chosen the more macro charges are in the calculation domain. Each emission point emits a fraction of a bunch charge during the emission time at discrete time steps. Fig. 7 shows a circular source with the dots representing emission points. Macro charges in the transverse plane as well as along the axis z are distributed according to the Gaussian function $f(x) = (1/\sqrt{2\pi}\sigma)exp(-x^2/2\sigma^2)$, where x is the emission circle radius for the transverse charge distribution, and the longitudinal coordinate (z) for the longitudinal charge distribution; σ is RMS width of the bunch charge density, defined separately for the longitudinal and transverse distributions.

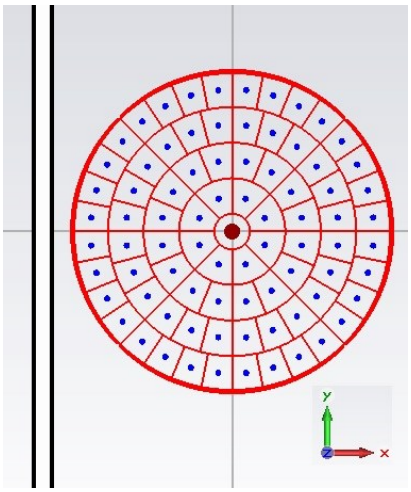

Fig. 7 Scheme of a circular charge emission. 81 blue dots are emission points.

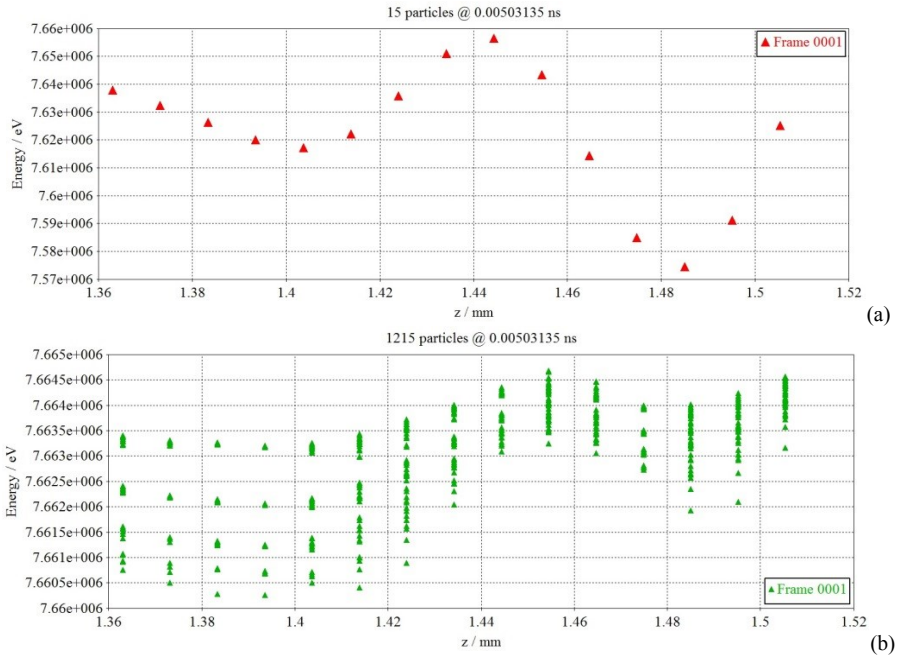

Fig. 8 Longitudinal distribution of bunch with σ_{long} = 0.1mm in the calculation domain. (a) Point-like charge propagation along the axis z, red marks represent energy of macro charges emitted by a single emission point. (b) Circular source with σ_{transv} = 0.9 mm represented by 1215 macro particles emitted from 81 emission points.

Fig. 8 shows the mechanism of macro-charges emission along the axis z for a point-like and a Gaussian-distributed bunch with σ_{long} = 0.1mm and σ_{transv} = 0.9 mm, 15 longitudinal slices are shown. In the case of point-like emission, Fig. 8(a), the bunch charge is represented by 15 macro particles, and in the case of Gaussian-like emission, Fig. 8(b), 1215 macro-particles are introduced in the calculation domain.

Fig. 9 demonstrates SPR radiation intensity dependence on the polar angle Theta for various emission source sizes. It shows that radiation intensity decreases with the growing size of the emission source. Similar dependence between the bunch transverse size and the emitted radiation intensity, transverse suppression effect, is characteristic of a field distribution at the exit of an undulator, discussed in [14].

One may note that there is no significant widening of the radiation distribution. Oscillations on the sides of the SPR peaks and at the angles Theta in the region 40 to 60 deg., which come from calculation errors, are significantly reduced. This take place in the case of the Gaussian bunch when for multiple emission sources each one of them is contained within its own mesh cell, or at least the emission area is defined by multiple mesh cells, on the contrary only one mesh cell defines a point-like emission source. Therefore, definition of a Gaussian like emission area in the transverse plane leads to a reduced calculation error.

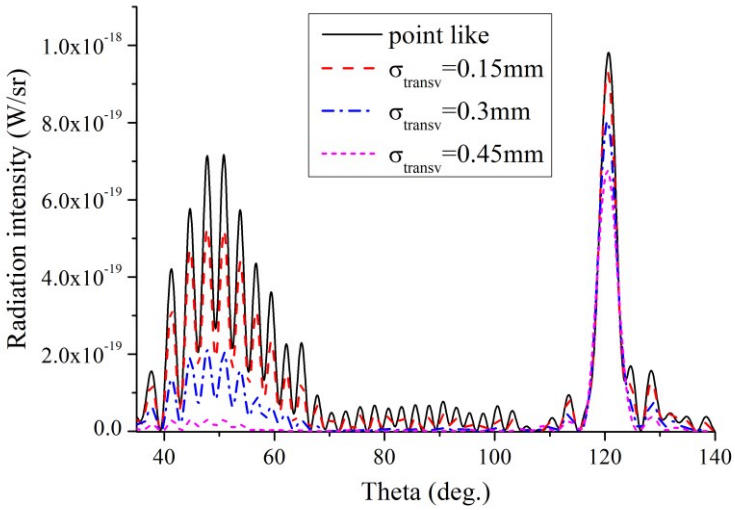

Fig. 9 SPR polar distribution. Parameters: Phi = 0; transverse size is from a point-like source to $\sigma_{transv} = 0.45$mm; $\gamma = 16$; d = 0.1 mm; h = 0.7 mm.

3.4 SPR intensity dependence on the bunch Lorentz factor and the grating strip depth.

In [15] the authors performed comparison between van den Berg's [16], Surface current [17, 18], and Resonant Diffraction Radiation (RDR) models of SPR from gratings of various profiles. One of the criteria for models verification was to compare the SPR intensity dependence on Lorentz factor. According to Van den Berg's model, an increase of a particle energy leads to decrease of the SPR yield, on the contrary Surface current and RDR theory predict radiation decrease. In [15] dependencies on Lorentz factor for a flat grating (d/p= 0.001) and a vertical strip grating (w1/p = 0.001) were calculated based on RDR theory, that predicted radiation increase while the Lorentz factor was increasing, and for Van den Berg's model showing the opposite behavior.

It was interesting to verify those results by simulating SPR intensity dependence on the bunch Lorentz factor for the strips with similar geometrical characteristics: horizontal strips (d/p = 0.1) and vertical strips (w1/p = 0.2). Despite the fact that characteristic ratios d/p and w1/p in the simulations do not match exactly the theoretical ratios mentioned earlier, simulated ones being two orders of magnitude larger, in Fig.10 one may observe that the simulation results are in agreement with RDR theory. For both horizontal strip and vertical strip gratings, the SPR intensity increases until the value of gamma reaches 15, and, then, the value of the radiation intensity maintains almost the same value in the range of Lorentz factors used in the simulation. Similar dependence was demonstrated in [15] for RDR theory.

In the experimental work [19] it was shown that for a lamellar grating, the electron beam with $\gamma = 78$ and the wavelength of a few millimeters, one can observe a periodic behavior of the radiation intensity depending on a chosen grating depth. In [19] a three – dimensional theoretical problem was solved for lamellar grating using the modal expansion method applied to van den Berg's model. The experimental results showed a reasonable agreement with the theoretical study, which identified a periodic behavior of the sum of electric and magnetic fields squared as a function of the grating groove depth. For both the theory and the experiment the period of SPR intensity oscillations was approximately equal to the value of λ/2, where λ is the observation wavelength. This result is also in agreement with earlier theoretical work discussed in [20].

Similar behavior was identified in the simulations for THz frequency region. In Fig. 11 SPR intensity dependence on the grating depth is obtained for three wavelengths 0.5, 0.6 and 0.67 mm, corresponding to the frequencies 600, 500 and 450GHz. One may clearly see a periodic dependence with the period approximately equal to the value of λ/2. The experimental and the theoretical dependencies in [19] demonstrated maxima of SPR intensity at the small grating depths, corresponding to the case of a shallow grating. For the simulated curves in Fig. 11 there is a gradual periodic decrease of the radiation intensity towards larger grating depths, and similarly to the experimental study [19] the maximum of SPR intensity is achieved at small grating depths near the value of λ/4.

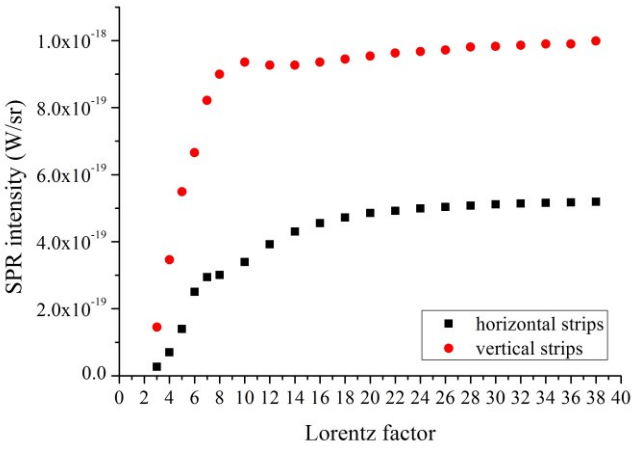

Fig. 10 SPR intensity dependence on Lorentz factor. Parameters: Phi = 0; Theta correspond to the peak of SPR distribution ($n = -1$); $\sigma_{transv} = 0.3$mm; γ = 16; d = 0.04mm (horizontal strip); d = 1mm (vertical strip); h = 0.5 mm.

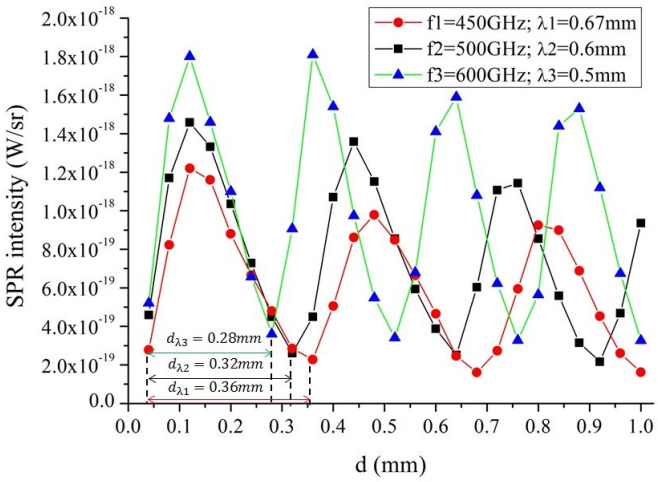

Fig. 11 SPR intensity dependence on grating depth. Parameters: Phi = 0; Theta correspond to the peak of SPR distribution ($n = -1$); $\sigma_{transv} = 0.3$mm; γ = 16; h = 0.5 mm.

4. Conclusions

CST PIC solver was tested as a tool for simulation of SPR from lamellar profile grating with vacuum gaps. Meshing study was performed, and the limits of stable calculations were identified in terms of the discretization ration for a given frequency. Effects of the transverse bunch size on the calculation accuracy and on the SPR peak width and intensity were investigated. It was shown that definition of a Gaussian-distributed bunch in the transverse plane by multiple emission points reduces calculation error.

Polar and azimuthal SPR distributions were compared with the RDR theory on a relative scale. Very good agreement in terms of the peak position and width was shown for the polar radiation distribution. However, some widening of the azimuthal radiation distribution was observed, which could be caused by the fact that RDR theory was developed for strips with infinite transverse dimensions, while the simulated distribution was obtained for a fixed transverse size of strips. As a consecutive step of this investigation, in the future work it will be interesting to compare the obtained results with other models of Smith-Purcell radiation developed in [16, 17, 21].

Once the influence of the meshing effects and the emission source sizes on the radiation and spectral distributions was confirmed, and reasonable agreement of the simulations with RDR theory was achieved, CST PIC solver was tested as a tool for SPR grating optimization. The SPR intensity dependence on Lorentz factor was calculated for the horizontal and vertical strip gratings, qualitative agreement with RDR theory was confirmed. SPR intensity dependence on groove depth was investigated for THz frequencies, oscillating dependence with gradually decreasing intensity towards larger grating depths was observed. The period of the oscillations was approximately equal to the value of λ/2 and the maximum of SPR intensity was located at the small grating depths near to the value of λ/4. Similar behavior with the maximum of SPR intensity at small grating depths and the periodic intensity dependence with the period of approximately λ/2 was observed and theoretically explained in [19] for the mm wavelength range.

References

1. T. Kampfrath, K. Tanaka and K.A. Nelson, Resonant and nonresonant control over matter and light by intense terahertz transients, Nature Photonics 7 (2013) 680.
2. D.M. Mittleman, Frontiers in terahertz sources and plasmonics, Nature Photonics 7 (2013) 666.
3. A.P. Potylitsyn, M.I. Ryazanov, M.N. Strikhanov, Diffraction Radiation from Relativistic Particles, Springer, 2011.
4. S.E. Korbly et al., Observation of frequency-locked coherent Terahertz Smith-Purcell radiation, PRL 94 (2005) 054803.
5. A.S. Kesar et al., Power measurements of frequency locked Smith-Purcell radiation, PRSTAB 9 (2006) 022801.
6. M. Fukuda et al., Upgrade of the accelerator for the laser Undulator compact X-ray source (LUCX), NIMA 637 (2011) S67.

7. A. Aryshev et al., Development of advanced THz generation schemes at KEK LUCX facility, Proc. PASJ, Japan (2013).
8. K.V. Lekomtsev, A.S. Aryshev, P.V. Karataev, M.V. Shevelev, A.A. Tishchenko and J. Urakawa, Simulations of Transition Radiation from a Flat Target using CST Particle Studio, J. Phys.: Conf. Ser. 517, (2014) 012016.
9. http://www.cst.com/Content/Products/PS/Overview.aspx
10. T. Weiland, A discretization method for the solution of Maxwell's equations for six - component fields, Electronics and Communication (AEU) 31 (1977) 116
11. T. Weiland, Time domain electromagnetic field computation with finite difference methods, INTERNATION JOURNAL OF NUMERICAL MODELLING: ELECTRONIC NETWORKS, DEVICES AND FIELDS 9 (1996) 295
12. A.P. Potylitsyn, Smith-Purcell effect as resonant diffraction radiation, NIMA 145 (1998) 60.
13. K.S. Yee, D. Ingham and K. Shlager, Time-Domain Extrapolation to the far field based on FDTD calculations, IEEE Transactions of Antennas and Propagation Vol. 39 No. 3 (1991) 410.
14. E.L. Saldin, E.A. Schneidmiller, M.V. Yurkov, A simple method for determination of the structure of ultrashort relativistic electron bunches, NIM A 539 (2005) 499.
15. D.V. Karlovets and A.P. Potylitsyn, Comparison of Smith-Purcell radiation models and criteria for their verification, PRSTAB 9 (2006) 080701.
16. P.M. van den Berg, Smith-Purcell radiation from a point charge moving parallel to a reflection grating, Journal of the Optical Society of America 63 (1973) 1588.
17. J. Walsh, K. Woods and S. Yeager, Intensity of Smith-Purcell radiation in the relativistic regime, NIM A 341 (1994) 277
18. J.H. Brownell, J. Walsh and G. Doucas, Spontaneous Smith-Purcell radiation described through induced surface currents, Phys. Rev. E 57 (1998) 1075
19. Y. Shibata et al., Coherent Smith-Purcell radiation in the millimeter-wave region from a short bunch beam of relativistic electrons, Phys. Rev. E Vol. 57 N.1 (1998) 1061.
20. O.A. Tret'yakov, E.I. Chernyakov and V.P. Shestopalov, Theory of the Smith-Purcell effect, Izvestiya VUZ. Radiofizika, Vol. 9, No. 2 (1966) 341.
21. V.P. Shestopalov, Smith-Purcell effect, Nova Biomedical USA, 1998.